Initial Studies with ^{11}C-Vorozole PET Detect Overexpression of Intratumoral Aromatase in Breast Cancer

Anat Biegon[1], Kenneth R. Shroyer[2], Dinko Franceschi[1], Jasbeer Dhawan[1], Mouna Tahmi[1], Deborah Pareto[3], Patrick Bonilla[4], Krystal Airola[1], and Jules Cohen[5]

[1]Department of Radiology, Stony Brook University School of Medicine, Stony Brook, New York; [2]Department of Pathology, Stony Brook University School of Medicine, Stony Brook, New York; [3]Radiology Department, Vall d'Hebron University Hospital, Barcelona, Spain; [4]Department of Obstetrics and Gynecology, Nassau University Medical Center, East Meadow, New York; and [5]Hematology/Oncology, Stony Brook University School of Medicine, Stony Brook, New York

Aromatase inhibitors are the mainstay of hormonal therapy in estrogen receptor–positive breast cancer, although the response rate is just over 50% and in vitro studies suggest that only two thirds of postmenopausal breast tumors overexpress aromatase. The goal of the present study was to validate and optimize PET with ^{11}C-vorozole for measuring aromatase expression in postmenopausal breast cancer in vivo. **Methods:** Ten newly diagnosed postmenopausal women with biopsy-confirmed breast cancer were administered ^{11}C-vorozole intravenously, and PET emission data were collected between 40 and 90 min after injection. Tracer injection and scanning were repeated 2 h after ingestion of 2.5 mg of letrozole. Mean and maximal SUVs and ratios to nontumor tissue in the contralateral breast were determined at baseline and after letrozole. Biopsy specimens from the same tumors were stained for aromatase using immunohistochemistry and evaluated for stain intensity and the percentage of immune-positive cells. **Results:** Seven of the 10 women (70%) demonstrated increased mean focal uptake of tracer (SUV ratio $>$ 1.1) coinciding with the mammographic location of the lesion, whereas the other 3 women (30%) did not (SUV ratio $\leq$ 1.0). All patients with an SUV ratio above 1.1 had mean SUVs above 2.4, and there was no overlap (SUV ratio $\leq$ 1; SUV_{mean}, 0.8–1.8). The SUV ratio relative to breast around tumor was indistinguishable from the ratio to contralateral breast. Pretreatment with letrozole reduced tracer uptake in most subjects, although the percentage of blocking varied across and within tumors. Tumors with a high SUV in vivo also showed a high immunohistochemical staining intensity. **Conclusion:** PET with ^{11}C-vorozole is a useful technique for measuring aromatase expression in individual breast lesions, enabling noninvasive quantitative measurement of baseline and posttreatment aromatase availability in primary tumors and metastatic lesions.

Key Words: aromatase; cyp19A; breast cancer; PET; vorozole

J Nucl Med 2020; 61:807–813
DOI: 10.2967/jnumed.119.231589

Aromatase, a member of the cytochrome P450 protein superfamily, is a unique product of the *CYP19* gene (*1*). Aromatase catalyzes the last and obligatory step of estrogen biosynthesis. Aromatase expression and activity in the ovary (*2*) support estrogen synthesis for the classic endocrine model, but aromatase and additional enzymes and translocators necessary for local synthesis are also found in classic estrogen target organs such as breast, brain, bone, and adipose tissue (*3–6*). Local synthesis and use of estrogen (intracrinology) appear to be the dominant mode of estrogenic function in postmenopausal women (*7*), and there is increasing evidence that a significant proportion of postmenopausal breast tumors (~60%) overexpress aromatase independently of tumor histology and receptor status and are capable of synthesizing and using estrogen through this mechanism, with the intratumoral estrogen concentration up to an order of magnitude higher than the plasma or benign breast level (*8–13*). Recent studies on animal models have suggested that overexpression of aromatase is even more important than expression of dysregulated estrogen receptor (estrogen receptor-α) in the generation of mammary hyperplasia and cancer (*14*).

Although aromatase inhibitors (AIs) are among the most effective drugs currently used in the endocrine treatment of breast cancer, for reasons that are not fully understood the objective response rate is about 50% and predictors of responsiveness remain the subject of intense research and debate (*15–22*).

We have shown that ^{11}C-vorozole PET is a safe, sensitive, and selective noninvasive method for detection of physiologic aromatase expression in healthy human subjects (*5,23–26*). First labeled and used in rats and rhesus monkeys (*27,28*), a modified synthesis was later introduced, validated, and characterized in baboons (*29–31*) and the human brain (*32,33*). The present studies were undertaken to validate the use of this technique for identification of aromatase-overexpressing breast tumors. A new tool for noninvasive identification of aromatase overexpression in breast cancer may help select appropriate candidates for AI treatment and prevent unnecessary exposure to the adverse effects of AI, such as joint pain, hot flashes, and bone loss (*19*).

MATERIALS AND METHODS

Subjects

Between April 2015 and November 2016, 12 newly diagnosed postmenopausal women with breast cancer were prospectively recruited from the Carol Baldwin Breast Cancer Center at Stony Brook

Received May 24, 2019; revision accepted Oct. 30, 2019.
For correspondence or reprints contact: Anat Biegon, Department of Radiology, Stony Brook University School of Medicine, 101 Nicolls Rd., Stony Brook, NY 11794.
E-mail: anat.biegon@stonbrook.edu
Published online Nov. 22, 2019.

Medicine for a breast imaging study with ^{11}C-vorozole. Subjects were considered eligible if they were postmenopausal (≥50 y old and ≥12 mo from last menstrual period), had biopsy-confirmed breast cancer, had undergone mammography within 3 mo of study enrollment, and were able to provide written informed consent. Subjects were excluded if they had current or past treatment with AIs; current or recent use of hormone replacement therapy; or medical conditions likely to affect radiotracer uptake and image interpretation, including cardiovascular disease, breast surgery, and breast inflammation or infection. Subjects who were active smokers were excluded because our published findings indicate that tobacco alkaloids inhibit aromatase in vivo (*5,31*).

The institutional review boards and radioactive drug research committees of both institutions approved this study, and all subjects gave written informed consent.

Pharmacologic Properties of ^{11}C-Vorozole and Letrozole

S-vorozole (6-[(*S*)-(4-chlorophenyl)-1H-1,2,4-triazol-1-ylmethyl]-1-methyl-1H-benzotriazole) is a specific and potent (inhibitory constant, 0.7 nM) nonsteroidal, competitive AI. Originally developed as an antineoplastic agent, the compound is extensively metabolized by the liver and has an elimination half-life of 8 h.

Peak levels in tissue were achieved by 30 min, followed by stabilization over the 90-min acquisition. Metabolite-corrected plasma levels indicated a plasma half-life of more than 60 min (*32*). Kinetic modeling showed a similar rank order of target density in various brain regions using several analytic approaches, including a single tissue compartment, 2 tissue compartments, Logan plots, tissue-over-plasma ratios, and brain region–over–cerebellum ratios in primate and human brain (*30,33*).

As part of the tracer validation, 33 healthy subjects, 13 men and 20 women, were enrolled in a multiple-scan study, which entailed 2 visits and 4 scans per subject, including combinations of brain, body, retest, and blocking studies (*5*). There were no adverse or clinically detectable pharmacologic effects in any of the 33 subjects or the more than 100 scans performed.

Letrozole (Femara; Novartis) is a Food and Drug Administration–approved AI prescribed as an oral daily 2.5-mg dose for the treatment of breast cancer patients (*15*). Studies on healthy volunteers with a single dose of letrozole showed that this standard dose blocks close to 80% of aromatase activity and that the maximum concentration is reached within 2–2.5 h. The effect of a single dose of the drug (monitored by a decline in estrogen levels) peaks within 2–2.5 h of administration and lasts for more than 24 h (*16,17*). Using the same dose and time interval, we have previously shown, as part of the tracer validation process, that letrozole blocks ^{11}C-vorozole brain uptake (*5,29–33*).

PET Studies

Radiosynthesis was performed at Weill Cornell Biomedical Imaging Center using published methodology (*29–33*). Intravenous catheters were placed in both arms, one for radiotracer injection and the other for blood sampling.

Patients were placed prone on adjustable 2-piece foam cushion sets available in 3 sizes, allowing for a customized opening for the breasts to rest in a neutral position.

PET scanning was performed on a Siemens Biograph mCT–S 64-slice PET/CT time-of-flight tomograph at the Weil Cornell Medical College imaging center, as a 3-dimensional dynamic acquisition. A short (<1 min) nondiagnostic CT scan was obtained first for attenuation correction.

^{11}C-vorozole was injected as a fast, intravenous bolus. Radiochemical purity exceeded 99%, and the specific activity ranged from 72 to 185 MBq/μmol. The resulting injected mass was less than 1.7 μg/study, and the radioactive dose ranged from 148 to 296 MBq.

Forty minutes after injection, a dynamic PET image acquisition commenced and continued for 50 min (5 frames at 10 min each). At the end of the first scan, the subjects were given an oral dose of letrozole (2.5 mg), and a second injection of tracer was administered 2 h later, followed by a second CT and PET acquisition (blocking study).

PET images were reconstructed using the manufacturer's recommended method for this scanner (TrueX+TOF, ultraHD-PET; Siemens), consisting of an iterative reconstruction algorithm (2 iterations, 21 subsets) with both attenuation and scatter correction, a final image size of 200 × 200 pixels, and a voxel size of 4.07 × 4.07 × 3 mm.

The PET data were analyzed by an experienced PET and MRI biomedical physicist masked to the identity of the subject and the results of the mammography, using the PMOD program (PMOD Technologies LLC). The regions of interest were manually delimited with a freehand tool. A region of interest was placed around the apparent location of the lesion, and similarly sized regions of interest were also placed in the area adjacent to the lesion and in a similar anatomic location in the contralateral breast. In addition, we measured SUV in the whole contralateral breast. Region-of-interest size varied with the size of the individual tumors and breasts. Mean and SUV_{max} were calculated using the formula SUV = activity in region of interest (MBq per cm^3)/injected activity normalized for patient weight (MBq per kg). Subjects were encouraged to report any adverse effects. In addition, the study coordinator telephoned each subject within 24 h of the last scan to inquire about adverse effects.

Pathology

Histologic typing; tumor and tumor stage; and the estrogen receptor, progesterone receptor, human epidermal growth factor receptor type 2 (HER2), and Ki-67 status were determined by the standard method of the Diagnostic Histology Laboratory of the Department of Pathology. Cutoffs for estrogen receptor and progesterone receptor were at least 1% tumor cells (*34*). HER2 immunohistochemistry test results of 3+ were scored as positive according to the HercepTest Interpretation Manual (Dako) (*35*). HER2 test results of 2+ were scored as equivocal and prompted fluorescence in situ hybridization testing, for which a ratio of more than 2.0 for HER2 copy number to CEP17 control was considered positive.

Aromatase Immunohistochemistry

At least 2 slides from each patient specimen, containing tumor and adjacent benign breast tissue, were processed for aromatase immunohistochemistry using a goat-antihuman polyclonal antibody to aromatase from LifeSpan BioSciences, Inc.—a method that has been shown to produce high-quality staining (*11*). The tissue preprocessing and staining protocol was optimized through adaptations of the manufacturer's protocol.

Tissue specimens used for method optimization and validation were obtained under institutional review board approval from the archival collections of formalin-fixed, paraffin-embedded blocks at the State University of New York at Stony Brook, Department of Pathology, between 2004 and 2008.

The tissue preprocessing and staining protocol was adapted from the manufacturer's protocol to maximize signal intensity and specificity (Supplemental Fig. 1; supplemental materials are available at http://jnm.snmjournals.org) by testing different reagents, temperatures, and durations of incubation in the presence and absence of the primary antibody, first on placenta tissue, known to express high levels of aromatase, and then on normal breast and breast tumor tissue. Subsequently, a positive (human placenta) and negative (primary antibody omitted) control slide were processed in conjunction with each staining experiment.

The optimized protocol involved sectioning of tumor and benign breast tissues at 4 μm, mounting on charged glass slides (SuperFrost

Plus; Thermo Fisher Scientific), and baking overnight at 60°C. The slides were deparaffinized in xylene and rehydrated through graded alcohols. Endogenous peroxidase activity was blocked by a 5-min treatment with 3.0% hydrogen peroxide and antigen retrieval by heating the slides to 120°C for 10 min in 20 mM citrate buffer (pH 6.0). The slides were then incubated with aromatase antibody diluted 1:1,000 at room temperature for 60 min, followed by visualization through an indirect avidin-biotin–based immunoperoxidase method, using a Vectastain Elite ABC kit (Vector Laboratories). Subsequently, the sections were developed using 3,3′-diaminobenzidine, counterstained with hematoxylin, and then dehydrated in graded alcohols, after which a coverslip was applied. For each batch, the immunohistochemistry staining was revalidated using positive and negative controls (Supplemental Fig. 1).

Immunohistochemistry Data Analysis

An experienced pathologist reviewed the entire section at a magnification of ×100 and estimated the percentage of aromatase-positive tumor cells and the staining intensity, which ranged from 0 (negative) to 3 (high intensity).

Quantitative Analysis of Stained Cells

Digital photographs of stained slides (×400 magnification) were quantitatively analyzed using ImageJ (National Institutes of Health) software (Supplemental Fig. 1). The total numbers of cells (hematoxylin-stained nuclei) and aromatase (3,3′-diaminobenzidine)-positive cells were counted using unbiased stereologic principles (minimum, 100 cells; 3 fields). Subsequently, the images were deconvoluted to separate the 3,3′-diaminobenzidine signal from the hematoxylin and eosin signal, and the 3,3′-diaminobenzidine signal density was measured in at least 100 cells per subject to assess changes in aromatase expression per cell.

Semiquantitative Analysis of Malignant Cells

An experienced pathologist reviewed the entire section at a magnification of ×100 and scored the percentage of aromatase-positive malignant cells (0–100) and the staining intensity on a scale of 0 (none) to 3 (high intensity).

Statistics

Statistical analyses were performed using Statview software (Abacus). ANOVA was used to examine the effects of diagnostic group, region of interest, time of tracer uptake or immunohistochemical parameters. Analyses yielding a significant main effect were followed by Fisher post hoc least significant difference analysis with an α preset of 0.05.

RESULTS

Subject Disposition

The first of the 12 consenting subjects was not scanned because of a radiosynthesis failure, the eighth was not scanned because of a scheduling failure, and 1 subject (subject 9, Supplemental Table 1) received only a single (baseline) scan because of injection failure (collapsed vein) in the postletrozole (blocking) study. Thus, 10 women had baseline scans with ^{11}C-vorozole, and 9 had both baseline and blocking studies. Venous blood collection for kinetics and metabolite analysis was attempted but not completed in most subjects for technical reasons (poor veins, equipment problems).

Patients ranged from 54 to 75 y old (median age, 63 y) and weighed between 59 and 113 kg (median weight, 79 kg). Six patients had invasive ductal carcinoma, 3 had invasive lobular carcinoma (2 classic type, 1 pleomorphic), and 1 had a mixed ductal and lobular histology. Eight patients had early-stage breast cancer (stages I–III), and 2 had metastases to distant organs (stage IV). Seven patients were estrogen receptor–positive, 3 were estrogen receptor–negative, and 4 were HER2-positive (Supplemental Table 1).

There were no adverse effects (e.g., flushing, itching, or injection site reaction) reported or observed in any of the 10 participants or 19 scans.

Visual inspection of the ^{11}C-vorozole PET images (averaged emission data collected between 40 and 90 min after tracer administration) revealed 3 distinct profiles (Fig. 1). In 6 of 10 patients, high focal uptake was observed at baseline, localized to the mammographic location of the tumor (arrow), and this uptake was decreased in tumor and heart after letrozole administration (Fig. 1A). Three of the 10 patients did not have a focal increase in uptake at the tumor location (Fig. 1B). One patient with highly metastatic cancer had high though heterogeneous focal uptake at the location of the primary tumor (Fig. 1D). Multiple bone metastases and a high-uptake area adjacent to the primary tumor (node 2) were observed in the same patient (Figs. 1C and 1D). Letrozole administration did not result in an appreciable decrease in uptake in this patient.

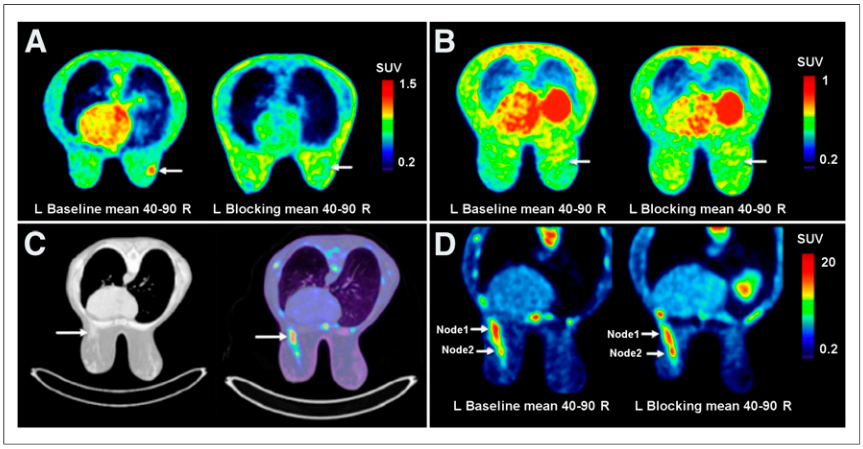

FIGURE 1. Aromatase availability imaged by ^{11}C-vorozole in women with breast cancer. (A) SUV map from patient with single lesion on mammography (arrow) before and after letrozole administration (blocking). Focal uptake is seen in tumor area at baseline, and decreased uptake is seen in tumor and heart. This pattern was observed in 6 of 10 patients. (B) SUV map from patient with single lesion on mammography (arrow), which did not show increased tracer uptake. This pattern was seen in 3 women. (C) CT (left) and PET overlaid on CT (right) from patient with stage IV metastatic cancer. Arrow indicates location of primary tumor on patient's mammogram. (D) SUV maps of same patient. Node 1 arrow points to location and size identified on mammography. Multiple bone metastases and high-uptake area adjacent to primary tumor (node 2) can be seen with no apparent blocking.

PET data analysis in nontumor regions showed similar mean SUVs in the whole contralateral breast, perilesional breast tissue (around the tumor), and an area in the contralateral breast corresponding in location and size to the primary tumor (mean ± SD: 1.89 ± 0.5, 1.87 ± 0.53, 1.9 ± 0.48, respectively). In 7 (70%) of the 10 women scanned, SUV_{mean} in the area coinciding with the mammographic location of the

TABLE 1
^{11}C-Vorozole Uptake in Tumor Area Before and After Letrozole

Number	Lesion SUV_{mean}	Lesion SUV_{max}	% block mean	SUVR mean
2	13.69	24.43	0	5.87
3	4.66	6.03	21.8	2.84
4	5.80	7.83	20.1	2.75
5	1.61	3.80	25.7	0.92
6	0.79	1.41	0	1.00
7	3.63	4.86	53.3	1.44
9	2.47	3.03	NA	1.91
10	1.78	4.40	3	1.01
11	3.20	4.09	56.3	1.80
12	2.61	3.98	18.9	1.73

%block = 100 − [(SUV after letrozole/SUV baseline) × 100]; NA = not available, no blocking study performed.

lesion was increased by 10% or more relative to perilesional and contralateral breast regions of interest (SUV ratio > 1.1; Fig. 1; Table 1). The other 3 women (30%) did not show increased uptake in the tumor (SUV ratio ≤ 1.0). All subjects with an SUV ratio above 1.1 had SUVs above 2.4, and there was no overlap in SUV between the 2 groups (Table 1), with SUV_{mean} in tumors overexpressing aromatase (SUV ratio > 1.1) ranging from 2.47 to 13.6, whereas SUV_{mean} in tumors not overexpressing aromatase (SUV ratio ≤ 1) ranged from 0.8 to 1.8. SUV ratio relative to breast around tumor was indistinguishable from the ratio to contralateral breast (mean ± SD: 2.17 ± 1.66 [range, 0.74–5.8] and 2.08 ± 1.57 [range, 0.74–5.5], respectively).

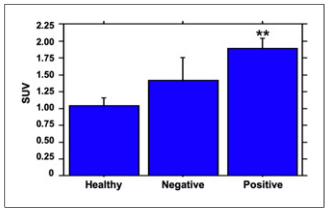

FIGURE 2. ^{11}C-vorozole uptake in breast tissue contralateral to aromatase-overexpressing and non–aromatase-overexpressing tumors and breasts of healthy women. Bars depict mean and SEM for each group. One-way ANOVA demonstrated significant main effect of group ($F_{2,14}$ = 5.94, P < 0.02). Fisher post hoc least significant difference test demonstrated highly significant difference (**P = 0.005) between healthy breasts (healthy, n = 5) and breasts contralateral to aromatase-overexpressing (positive, n = 7) lesion. Intermediate values, not significantly different from either group, were observed in breast tissue contralateral to aromatase-negative (negative, n = 3) lesions.

Of the 9 women rescanned after a single oral dose of letrozole, measurable blocking of tracer uptake (ranging from 3% to 53% of baseline), indicative of saturable and specific tracer binding, was observed in 7.

In addition, the SUVs of the whole contralateral breast from patients were compared with values from a group of 5 healthy postmenopausal volunteers (mean age, 57.8 ± 4.9 y) whose breasts were scanned under a previous protocol using the same tracer and conditions (*5*). Tracer uptake in breasts contralateral to an aromatase-positive lesion was significantly higher than uptake in the breasts of subjects without breast cancer (Fig. 2), whereas the SUVs in breasts contralateral to tumors not overexpressing aromatase were between the 2 groups and not statistically significantly different from either (Fig. 2).

Finally, mean SUVs were compared across frames and frame combinations to assess the feasibility of shortening the acquisition time in future clinical studies. SUV_{mean} was stable between 40 and 90 min after injection such that a 20-min acquisition period between 40 and 60 min was sufficient to predict SUV over the maximal acquisition period (≤90 min) dictated by the tracer half-life (Fig. 3).

Immunohistochemistry

Using our optimized protocol, staining for aromatase gave a consistently high signal in placenta (positive control), with varying intensity in archival tumor and normal tissue specimens. There was no staining when the first antibody was omitted (Supplemental Fig. 1).

Biopsy specimens from aromatase-overexpressing tumors showed increased staining (percentage positive multiplied by intensity) on immunohistochemistry relative to those that did not overexpress aromatase (Fig. 4; Supplemental Table 2). When the patient group was split around the median value of SUV and we compared the percentage of aromatase-positive cells and the average staining density between the resulting low–^{11}C-vorozole uptake and high–^{11}C-vorozole uptake groups, there was a statistically significant difference in mean stain density between the high and low groups, whereas the difference in the percentage of aromatase-positive cells did not reach statistical significance (Fig. 5; Supplemental Table 2). These findings suggest that increased aromatase expression per cell is a major contributor to the increased PET signal.

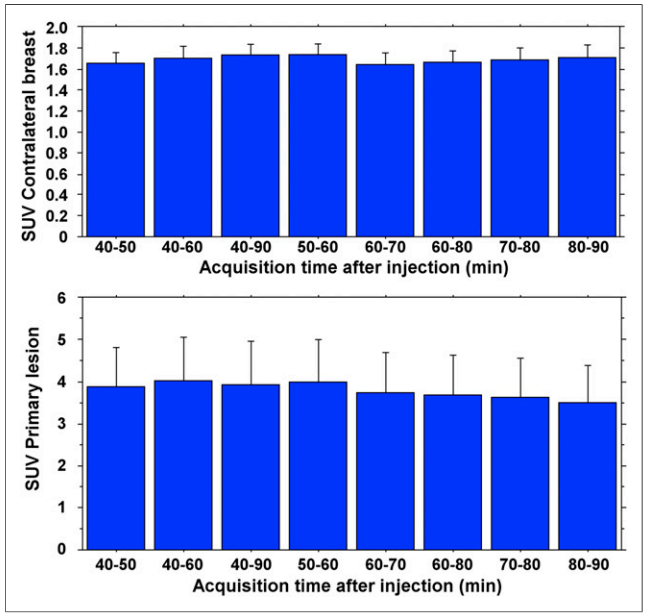

FIGURE 3. Mean tracer uptake in healthy breast and tumor over various intervals. Bars represent mean and SEM for 10 subjects (baseline scan). Emission acquisition began 40 min after tracer injection and continued for 50 min. SUV was averaged over entire acquisition (40–90 min) and several shorter intervals. There was no statistically significant difference (1-way ANOVA) among the various intervals.

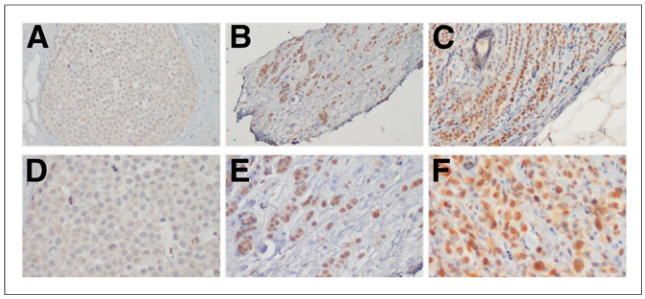

FIGURE 4. Immunohistochemical staining for aromatase in biopsy material from breast cancer patients imaged with ^{11}C-vorozole in vivo. (A and D) Patient with low-intensity labeling and low ^{11}C-vorozole uptake. (B and E) Patient with moderately high staining intensity and moderately high ^{11}C-vorozole uptake. (C and F) Patient with high staining intensity and high ^{11}C-vorozole uptake. Top row is ×200; bottom row is ×400.

DISCUSSION

The primary goal of this study was to validate and optimize the use of ^{11}C-vorozole PET in the noninvasive detection of aromatase-overexpressing tumors in a clinical breast cancer population before and after AI administration.

In the affected breast of 7 of 10 patients, ^{11}C-vorozole PET scans demonstrated increased focal uptake corresponding to the mammographic location of the primary tumor. The proportion of ^{11}C-vorozole–overexpressing tumors agrees well with published studies (on tissue specimens) reporting that approximately two thirds of postmenopausal breast tumors have increased aromatase expression and activity relative to healthy breast tissue (*3,9–11,13*). Tumor SUVs in these patients were also significantly higher than values obtained in healthy women (*5*), with no overlap. As expected from the literature (*3,9–11,13*), aromatase overexpression could not be predicted from any of the clinicopathologic markers routinely evaluated in breast cancer, including tumor type, stage, estrogen receptor expression, progesterone receptor expression, HER2 expression, or proliferation rate (Ki-67).

Interestingly, tracer uptake in the unaffected (contralateral) breast of breast cancer patients was higher than that in healthy women, suggesting that aromatase overexpression in nontumor tissue may be associated with an increased risk of breast cancer.

The 2 patients with no measurable blocking include the patient with the lowest SUV in this cohort and a patient with high-grade metastatic disease, who had the highest SUV in the group. There are several different potential reasons for the lack of inhibition in an individual patient, including accelerated metabolism or poor bioavailability of the blocking agent, genetic factors, or tumor-specific modifications of the aromatase enzyme (*36–40*). Interestingly, the patient with a high SUV began receiving neoadjuvant AI and died 6 mo after the scan, supporting the notion that aromatase overexpression alone might be necessary but not sufficient to predict responsiveness to AI therapy (*40*), which also requires target engagement by the drug at the planned dose. The remaining study participants were not subsequently treated with AIs before resection of their primary breast tumor.

The results of our study, including the feasibility of obtaining meaningful data within a relatively short and convenient acquisition window (40–60 min after injection), suggest that PET with ^{11}C-vorozole is a novel, unique, and useful technique for characterizing individual breast lesions, enabling, for the first time, noninvasive quantitative measurement of aromatase availability before and after AI exposure in primary and metastatic lesions. To date, the available methods of assessing aromatase expression, including immunohistochemistry, in situ hybridization, and enzyme activity assays, require material obtained after death or through invasive procedures. Immunohistochemistry is semiquantitative at best and is usually performed on limited material, such that false-negative results are likely, because of partial representation and tumor heterogeneity, as previously discussed in relation to estrogen receptor imaging with ^{18}F-fluoroestradiol (*41*).

Other PET tracers are currently used in clinical and research settings for breast cancer, most notably ^{18}F-FDG and ^{18}F-fluoroestradiol (*41–48*). The main advantage of PET over immunohistochemistry of biopsy specimens is that it provides quantitative in vivo assessment of all tumor sites throughout the body, an advantage shared by ^{11}C-vorozole. However, neither ^{18}F-FDG (*49,50*) nor ^{18}F-fluoroestradiol can provide direct information about the expression of intratumoral aromatase, which is increasingly implicated in the etiology, progression, and treatment of breast cancer (*3,9,10,14,36–40*)

The noninvasive nature of the procedure and the short half-life of the isotope also mean that ^{11}C-vorozole PET can be used repeatedly within the same day, enabling efficient clinical or investigational evaluation of target engagement and pharmacokinetics for novel and established AIs. The procedure can also be repeated periodically during the course of the disease, affording unprecedented access to long-term changes in aromatase expression in response to treatment and tumor evolution (*36–40*).

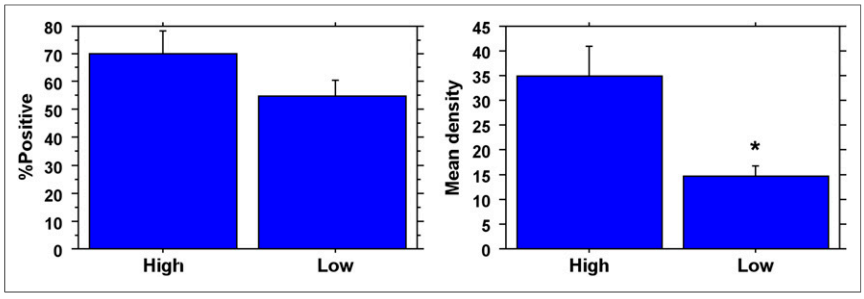

FIGURE 5. Quantitative immunohistochemical analysis of aromatase expression in patients with high and low vorozole uptake. (Left) Mean percentage of cells positively stained for aromatase among patients with high (above median, $n = 5$) and low (below median, $n = 5$) SUV. Difference was not statistically significant ($P = 0.2$). (Right) Mean staining intensity (density, 255 minus gray level) for aromatase among patients with high (above median, $n = 5$) and low (below median, $n = 5$) SUV. *$P < 0.02$, Student t test, 2-tailed.

Our study does have limitations, including the small size of the cohort and the limited number of health centers that produce ^{11}C-labeled radiopharmaceuticals. The only other aromatase tracer recently validated in healthy human subjects, ^{11}C-cetrozole (*51*), shares the same limitation. In addition, the study design, including cohort size and composition, does not fully address the possible contribution of ^{11}C-vorozole PET as a clinical companion diagnostic or predictor of AI treatment outcome. In this regard, our ongoing studies include investigation of ^{11}C-vorozole uptake and blocking in a cohort of patients with metastatic disease

who also had ^{18}F-FDG and MRI scans performed as part of their clinical workup. Future directions include testing the relationship between tumor response to AIs and pretreatment aromatase expression and blocking with commonly used AIs given for a slightly longer period (≤2 wk, to ensure steady state) (*52*), which will also include measurement of individual AI plasma levels, relevant polymorphisms in the aromatase gene (*36*), and the development and validation of AI diagnostic and theranostic radiopharmaceuticals labeled with isotopes with a longer half-life than ^{11}C (*53*).

CONCLUSION

PET with ^{11}C-vorozole is a useful technique for measuring aromatase expression in individual breast lesions, enabling noninvasive quantitative measurement of baseline and posttreatment aromatase availability in primary and metastatic lesions, an ability that can be used to enhance tumor characterization, patient selection, and treatment monitoring in breast cancer.

DISCLOSURE

This work was supported in part by NIH grant 1R01CA195506-01 (Jules Cohen and Anat Biegon, multiple principal investigators). No other potential conflict of interest relevant to this article was reported.

ACKNOWLEDGMENTS

We thank Drs. Alison Stopeck and Leah Baer of Stony Brook Medicine for help with subject recruitment, William Scherl for study coordination, and Shankar Vallabhajosula, PhD, and staff at the Citigroup Biomedical Imaging Center for tracer production and scan execution.

KEY POINTS

QUESTION: Is it possible to noninvasively visualize and measure aromatase availability in breast tumors in vivo?

PERTINENT FINDINGS: PET with ^{11}C-vorozole detected high focal uptake coinciding with the mammographic tumor location in 7 breast cancer patients. Biopsy material from all these tumors demonstrated a high density of aromatase immunohistochemical staining relative to 3 tumors that did not have high focal uptake of radiotracer.

IMPLICATIONS FOR PATIENT CARE: PET with ^{11}C-vorozole can be used to improve tumor characterization, treatment planning, and treatment monitoring in women with breast cancer considering hormonal treatment with AIs.

REFERENCES

1. Danielson PB. The cytochrome P450 superfamily: biochemistry, evolution and drug metabolism in humans. *Curr Drug Metab.* 2002;3:561–597.
2. Kragie L. Aromatase in primate pregnancy: a review. *Endocr Res.* 2002;28:121–128.
3. Brodie A, Lu Q, Nakamura J. Aromatase in the normal breast and breast cancer. *J Steroid Biochem Mol Biol.* 1997;61:281–286.
4. Simpson ER, Clyne C, Rubin G, et al. Aromatase: a brief overview. *Annu Rev Physiol.* 2002;64:93–127.
5. Biegon A, Alexoff DL, Kim SW, et al. Aromatase imaging with [N-methyl-^{11}C] vorozole PET in healthy men and women. *J Nucl Med.* 2015;56:580–585.
6. Rone MB, Fan J, Papadopoulos V. Cholesterol transport in steroid biosynthesis: role of protein–protein interactions and implications in disease states. *Biochim Biophys Acta.* 2009;1791:646–658.
7. Labrie F. All sex steroids are made intracellularly in peripheral tissues by the mechanisms of intracrinology after menopause. *J Steroid Biochem Mol Biol.* 2015;145:133–138.
8. McNamara KM, Sasano H. The intracrinology of breast cancer. *J Steroid Biochem Mol Biol.* 2015;145:172–178.
9. Lu Q, Nakmura J, Savinov A, et al. Expression of aromatase protein and messenger ribonucleic acid in tumor epithelial cells and evidence of functional significance of locally produced estrogen in human breast cancers. *Endocrinology.* 1996;137:3061–3068.
10. Di GH, Lu J, Song C, Li H, Shen Z, Shao Z. Over expression of aromatase protein is highly related to MMPs levels in human breast carcinomas. *J Exp Clin Cancer Res.* 2005;24:601–607.
11. Singer CF, Fink-Retter A, Gschwantler-Kaulich D, et al. Selective spatial upregulation of intratumoral stromal aromatase in breast cancer patients: evidence for imbalance of local estrogen metabolism. *Endocr Relat Cancer.* 2006;13:1101–1107.
12. Bulun SE, Simpson ER. Aromatase expression in women's cancers. *Innovative Endocrinology of Cancer.* New York, NY: Springer; 2008:112–132.
13. Geisler J, Suzuki T, Helle H, et al. Breast cancer aromatase expression evaluated by the novel antibody 677: correlations to intra-tumor estrogen levels and hormone receptor status. *J Steroid Biochem Mol Biol.* 2010;118:237–241.
14. Díaz-Cruz ES, Sugimoto Y, Gallicano GI, Brueggemeier RW, Furth PA. Comparison of increased aromatase versus ERα in the generation of mammary hyperplasia and cancer. *Cancer Res.* 2011;71:5477–5487.
15. Cohen MH, Johnson JR, Li N, Chen G, Pazdur R. Approval summary: letrozole in the treatment of postmenopausal women with advanced breast cancer. *Clin Cancer Res.* 2002;8:665–669.
16. Iveson TJ, Smith I, Ahern J, Smithers D, Trunet P, Dowsett M. Phase I study of the oral nonsteroidal aromatase inhibitor CGS 20267 in healthy postmenopausal women. *J Clin Endocrinol Metab.* 1993;77:324–331.
17. Buzdar AU, Robertson JF, Eiermann W, Nabholtz JM. An overview of the pharmacology and pharmacokinetics of the newer generation aromatase inhibitors anastrozole, letrozole, and exemestane. *Cancer.* 2002;95:2006–2016.
18. Santen RJ, Yue W, Naftolin F, Mor G, Berstein L. The potential of aromatase inhibitors in breast cancer prevention. *Endocr Relat Cancer.* 1999;6:235–243.
19. Smith IE, Dowsett M. Aromatase inhibitors in breast cancer. *N Engl J Med.* 2003;348:2431–2442.
20. Regan MM, Neven P, Giobbie-Hurder A, et al. Assessment of letrozole and tamoxifen alone and in sequence for postmenopausal women with steroid hormone receptor-positive breast cancer: the BIG 1-98 randomised clinical trial at 8.1 years median follow-up. *Lancet Oncol.* 2011;12:1101–1108.
21. Miron L, Negura L, Peptanariu D, Marinca M. Research on aromatase gene (CYP19A1) polymorphisms as a predictor of endocrine therapy effectiveness in breast cancer. *Rev Med Chir Soc Med Nat Iasi.* 2012;116:997–1004.
22. Moy I, Lin Z, Rademaker AW, Reierstad S, Khan SA, Bulun SE. Expression of estrogen-related gene markers in breast cancer tissue predicts aromatase inhibitor responsiveness. *PLoS One.* 2013;8:e77543.
23. Vanden Bossche H, Willemsens G, Roels I, et al. R 76713 and enantiomers: selective, nonsteroidal inhibitors of the cytochrome P450-dependent oestrogen synthesis. *Biochem Pharmacol.* 1990;40:1707–1718.
24. Koymans LM, Moereels H, Bossche HV. A molecular model for the interaction between vorozole and other non-steroidal inhibitors and human cytochrome P450 19 (P450 aromatase). *J Steroid Biochem Mol Biol.* 1995;53:191–197.
25. Johnston SR, Smith IE, Doody D, Jacobs S, Robertshaw H, Dowsett M. Clinical and endocrine effects of the oral aromatase inhibitor vorozole in postmenopausal patients with advanced breast cancer. *Cancer Res.* 1994;54:5875–5881.
26. de Jong PC, van de Ven J, Nortier HW, et al. Inhibition of breast cancer tissue aromatase activity and estrogen concentrations by the third-generation aromatase inhibitor vorozole. *Cancer Res.* 1997;57:2109–2111.
27. Lidström P, Bonasera TA, Kirilovas D, et al. Synthesis, in vivo rhesus monkey biodistribution and in vitro evaluation of a ^{11}C-labelled potent aromatase inhibitor:[N-methyl-^{11}C] vorozole. *Nucl Med Biol.* 1998;25:497–501.
28. Takahashi K, Bergström M, Frändberg P, Vesström E-L, Watanabe Y, Långström B. Imaging of aromatase distribution in rat and rhesus monkey brains with [^{11}C] vorozole. *Nucl Med Biol.* 2006;33:599–605.
29. Kim SW, Biegon A, Katsamanis ZE, et al. Reinvestigation of the synthesis and evaluation of [N-methyl-^{11}C] vorozole, a radiotracer targeting cytochrome P450 aromatase. *Nucl Med Biol.* 2009;36:323–334.
30. Pareto D, Biegon A, Alexoff D, et al. In vivo imaging of brain aromatase in female baboons: [^{11}C] vorozole kinetics and effect of the menstrual cycle. *Mol Imaging.* 2013;12(8).
31. Biegon A, Kim S-W, Logan J, Hooker JM, Muench L, Fowler JS. Nicotine blocks brain estrogen synthase (aromatase): in vivo positron emission tomography studies in female baboons. *Biol Psychiatry.* 2010;67:774–777.

32. Biegon A, Kim SW, Alexoff DL, et al. Unique distribution of aromatase in the human brain: in vivo studies with PET and [N-methyl-^{11}C] vorozole. *Synapse.* 2010;64:801–807.
33. Logan J, Kim SW, Pareto D, et al. Kinetic analysis of [^{11}C] vorozole binding in the human brain with positron emission tomography. *Mol Imaging.* 2014;13:1–12.
34. Yi M, Huo L, Koenig KB, et al. Which threshold for ER positivity? A retrospective study based on 9639 patients. *Ann Oncol.* 2014;25:1004–1011.
35. *HercepTestTM: Interpretation Manual—Breast Cancer.* Glostrup, Denmark: Dako; 2014.
36. Garcia-Casado Z, Guerrero-Zotano A, Llombart-Cussac A, et al. A polymorphism at the 3′-UTR region of the aromatase gene defines a subgroup of postmenopausal breast cancer patients with poor response to neoadjuvant letrozole. *BMC Cancer.* 2010;10:36.
37. Catalano S, Giordano C, Panza S, et al. Tamoxifen through GPER upregulates aromatase expression: a novel mechanism sustaining tamoxifen-resistant breast cancer cell growth. *Breast Cancer Res Treat.* 2014;146:273–285.
38. Milosevic J, Klinge J, Borg A-L, Foukakis T, Bergh J, Tobin NP. Clinical instability of breast cancer markers is reflected in long-term in vitro estrogen deprivation studies. *BMC Cancer.* 2013;13:473.
39. Shibahara Y, Miki Y, Ishida T, et al. Immunohistochemical analysis of aromatase in metastatic lymph nodes of breast cancer. *Pathol Int.* 2013;63:20–28.
40. de Jong PC, Blankenstein MA, Nortier JW, et al. The relationship between aromatase in primary breast tumors and response to treatment with aromatase inhibitors in advanced disease. *J Steroid Biochem Mol Biol.* 2003;87:149–155.
41. Peterson LM, Mankoff DA, Lawton T, et al. Quantitative imaging of estrogen receptor expression in breast cancer with PET and ^{18}F-fluoroestradiol. *J Nucl Med.* 2008;49:367–374.
42. Kumar R, Lal N, Alavi A. ^{18}F-FDG PET in detecting primary breast cancer [letter]. *J Nucl Med.* 2007;48:1751.
43. Çermik TF, Mavi A, Basu S, Alavi A. Impact of FDG PET on the preoperative staging of newly diagnosed breast cancer. *Eur J Nucl Med Mol Imaging.* 2008;35:475–483.
44. Basu S, Chen W, Tchou J, et al. Comparison of triple-negative and estrogen receptor-positive/progesterone receptor-positive/HER2-negative breast carcinoma using quantitative fluorine-18 fluorodeoxyglucose/positron emission tomography imaging parameters. *Cancer.* 2008;112:995–1000.
45. Lakhani P, Maidment AD, Weinstein SP, Kung JW, Alavi A. Correlation between quantified breast densities from digital mammography and ^{18}F-FDG PET uptake. *Breast J.* 2009;15:339–347.
46. Kumar R, Alavi A. Fluorodeoxyglucose-PET in the management of breast cancer. *Radiol Clin North Am.* 2004;42:1113–1122.
47. Lerman H, Metser U, Grisaru D, Fishman A, Lievshitz G, Even-Sapir E. Normal and abnormal ^{18}F-FDG endometrial and ovarian uptake in pre-and postmenopausal patients: assessment by PET/CT. *J Nucl Med.* 2004;45:266–271.
48. Liao GJ, Clark AS, Schubert EK, Mankoff DA. ^{18}F-fluoroestradiol PET: current status and potential future clinical applications. *J Nucl Med.* 2016;57:1269–1275.
49. Mortimer JE, Dehdashti F, Siegel BA, Trinkaus K, Katzenellenbogen JA, Welch MJ. Metabolic flare: indicator of hormone responsiveness in advanced breast cancer. *J Clin Oncol.* 2001;19:2797–2803.
50. Mankoff DA, Dunnwald LK, Gralow JR, et al. Blood flow and metabolism in locally advanced breast cancer: relationship to response to therapy. *J Nucl Med.* 2002;43:500–509.
51. Takahashi K, Hosoya T, Onoe K, et al. ^{11}C-cetrozole: an improved C-^{11}C-methylated PET probe for aromatase imaging in the brain. *J Nucl Med.* 2014;55:852–857.
52. Pfister CU, Martoni A, Zamagni C, et al. Effect of age and single versus multiple dose pharmacokinetics of letrozole (Femara®) in breast cancer patients. *Biopharm Drug Dispos.* 2001;22:191–197.
53. Erlandsson MKF, Takahashi K, Långström B. ^{18}F-labelled vorozole analogues as PET tracer for aromatase. *J Labelled Comp Radiopharm.* 2008;51:207–212.